Quantum Chemical Methods for Predicting and Interpreting Second-Order Nonlinear Optical Properties

Champagne, Benoît; Beaujean, Pierre; De Wergifosse, Marc; Hidalgo Cardenuto, Marcelo; Liégeois, Vincent; Castet, Frédéric

Published in:
Frontiers in Quantum Chemistry

DOI:
10.1007/978-981-10-5651-2_6

Publication date:
2018

Document Version
Publisher's PDF, also known as Version of record

Chapter 6
Quantum Chemical Methods for Predicting and Interpreting Second-Order Nonlinear Optical Properties: From Small to Extended π-Conjugated Molecules

Benoît Champagne, Pierre Beaujean, Marc de Wergifosse, Marcelo Hidalgo Cardenuto, Vincent Liégeois and Frédéric Castet

Abstract This chapter addresses the methodological and computational aspects related to the prediction of molecular second-order nonlinear optical properties, i.e., the first hyperpolarizability (β), by using quantum chemistry methods. Both small (reference) molecules and extended push-pull π-conjugated systems are considered, highlighting contrasted effects about (i) the choice of a reliable basis set together with the convergence of β values as a function of the basis set size, (ii) the amplitude of electron correlation contributions and its estimate using wave function and density functional theory methods, (iii) the description of solvent effects using implicit and explicit solvation models, (iv) frequency dispersion effects in off-resonance conditions, and (v) numerical accuracy issues. When possible, comparisons with experiment are made. All in all, these results demonstrate that the calculations of β remain a challenge and that many issues need to be carefully addressed, pointing out difficulties toward elaborating black-box and computationally cheap protocols. Still, several strategies can be designed in order to achieve a targeted accuracy, either for reference molecules displaying small β responses or for molecules presenting large β values and a potential in optoelectronics and photonics.

B. Champagne (✉) · P. Beaujean · M. de Wergifosse · M.H. Cardenuto · V. Liégeois
Laboratoire de Chimie Théorique, Unité de Chimie-Physique Théorique et Structurale, Université de Namur, rue de Bruxelles 61, 5000 Namur, Belgium
e-mail: benoit.champagne@unamur.be

M.H. Cardenuto
Instituto de Física, Universidade de São Paulo, 66318, 05314-970 São Paulo, SP, Brazil

F. Castet
UMR 5255 CNRS, Institut des Sciences Moléculaires (ISM), Université de Bordeaux, Cours de la Libération, 351, 33405 Talence Cedex, France

M.J. Wójcik et al. (eds.), *Frontiers of Quantum Chemistry*,
https://doi.org/10.1007/978-981-10-5651-2_6

Keywords First hyperpolarizability • Wave function versus density functional theory methods • Solvation models • Frequency dispersion • Basis sets

6.1 Introduction

The molecular properties known as the (electric dipole) polarizability (α), first (β) and second (γ) hyperpolarizabilities, are defined by a phenomenological equation describing the change in the electric dipole moment that results from the application of external electric fields:

$$\Delta\mu_\zeta = \sum_{\eta}^{x,y,z} \alpha_{\zeta\eta}(-\omega_\sigma;\omega_1)F_\eta(\omega_1) + \frac{1}{2!}\sum_{\eta,\chi}^{x,y,z} \beta_{\zeta\eta\chi}(-\omega_\sigma;\omega_1,\omega_2)F_\eta(\omega_1)F_\chi(\omega_2) + \frac{1}{3!}\sum_{\eta,\chi,\xi}^{x,y,z} \gamma_{\zeta\eta\chi\xi}(-\omega_\sigma;\omega_1,\omega_2,\omega_3)F_\eta(\omega_1)F_\chi(\omega_2)F_\xi(\omega_3) + \ldots \quad (6.1)$$

where $F_\eta(\omega_1)$ is the amplitude of the field oscillating at pulsation ω_1 and applied in the η direction and $\omega_\sigma = \sum_i \omega_i$. For more than a century in the case of the polarizability and half of that period for the higher-order responses, these properties have been the topic of intense activities among theoretical chemists and physicists. On the one hand, efforts have been devoted to the very accurate evaluation of these properties for atoms (i.e., α and γ because β is zero by symmetry) and small molecules with the aim of providing reference values for experiments, which usually rely on relative rather than on absolute measurements [1, 2]. This has stimulated extensive methods developments to account for electron correlation effects, frequency dispersion, vibrational contributions, as well as solvent effects. Small systems are also ideal to assess the reliability of new quantum chemistry methods because of reduced needs in computational resources. On the other hand, owing to their potential for achieving large nonlinear optical (NLO) responses, organic and mixed organic–inorganic chromophores were also the object of a large number of theoretical investigations, which allowed establishing structure–property relationships [3, 4]. These theoretical guidelines allowed designing molecular systems for applications in photonics and sensing devices, as well as for bio-imaging [5, 6].

This chapter discusses the use of quantum chemistry methods to calculate and interpret the NLO responses from small molecules to extended push-pull π-conjugated systems. This topic being very broad, the focus is restrained to the first hyperpolarizability rather than to both the first and second hyperpolarizabilities, and to the electronic response, leaving the pure vibrational and zero-point vibrational average counterparts for another contribution. Then, such quantum chemistry applications are illustrated in domains recently tackled by the authors. In particular, the discussion focuses on quantities that can be extracted from experimental

measurements, namely the hyper-Rayleigh scattering (HRS) hyperpolarizability, β_{HRS}, and the associated depolarization ratios (DR), or the electric field-induced second harmonic generation (EFISHG) response, $\beta_{//}$. The expressions of the HRS responses involve ensemble averages over the molecular orientations:

$$\beta_{HRS}(-2\omega;\omega,\omega) = \sqrt{\left\{\langle\beta_{ZZZ}^2\rangle + \langle\beta_{ZXX}^2\rangle\right\}} \tag{6.2}$$

$$DR = \frac{\langle\beta_{ZZZ}^2\rangle}{\langle\beta_{ZXX}^2\rangle} \tag{6.3}$$

in which X and Z are axes of the laboratory frame. The expressions of $\langle\beta_{ZZZ}^2\rangle$ and $\langle\beta_{ZXX}^2\rangle$ in terms of Cartesian molecular tensor components can be found in Ref. [7]. The EFISHG response corresponds to the projection of the vector part of β on the dipole moment vector:

$$\beta_{//}(-2\omega;\omega,\omega) = \frac{1}{5}\sum_i \frac{\mu_i}{|\vec{\mu}|}\sum_j (\beta_{ijj} + \beta_{jij} + \beta_{jji}) = \frac{3}{5}\sum_i \frac{\mu_i\beta_i}{|\vec{\mu}|} \tag{6.4}$$

6.2 Small Molecules in Gas Phase

A first element for accurately predicting the responses of small molecules is the selection of a sufficiently flexible atomic basis set, generally containing many polarization and diffuse functions. Diffuse functions are needed because a substantial part of the response originates from the outer and most diffuse part of the electron density. The need for polarization functions can easily be understood by noticing that the successive first-, second-, … order responses of a spherical (*s*) atomic orbital to an external field can be described by *p*-like, *d*-like, … functions. So, some authors have privileged adding selected diffuse and/or diffuse polarization functions to basis sets employed for geometry optimizations and thermodynamics [8–10]. Others have designed property-oriented basis sets [11, 12] or have used basis sets constructed by adding even-tempered sets of diffuse functions to the correlation consistent basis sets of Dunning and co-workers [13], showing that with multiple-augmented sets the electrical properties of small molecules converge smoothly [14]. This is illustrated in Fig. 6.1 for the main static β tensor components of the water molecule, calculated at the Hartree–Fock level. Alternatives to these atomic basis set approaches consist in employing a fully numerical approach [15, 16].

Then, electron correlation should be included at a sufficiently high level of approximation to achieve quantitative accuracy. Several levels of approximation and techniques are available. The easiest technique consists in calculating β from finite differentiation of the field-dependent energy of the molecule. This is the finite

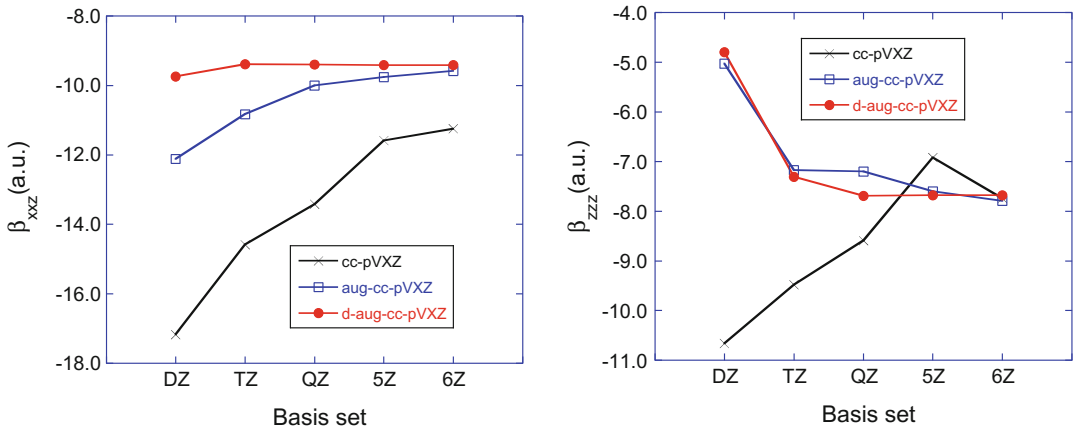

Fig. 6.1 Evolution of the amplitude of the two dominant components of the static β tensor of the water molecule calculated at the coupled-perturbed HF level by using the cc-pVXZ, aug-cc-pVXZ, and d-aug-cc-pVXZ basis set suites

field (FF) method [17] that simply requires adding the electric dipole interaction term, $-\hat{\mu}\cdot\vec{E}$, to the Hamiltonian. Still, the field amplitudes have to be carefully chosen within a stability window to avoid two drawbacks: (i) Too small field amplitudes create a loss of accuracy on the energy values, which gets amplified during the successive numerical derivatives, and (ii) too large field amplitudes introduce high-order contaminations in the derivatives before leading to divergences as a result of the change of the ground state electron configuration [18]. Nevertheless, once the stability window is defined, the high-order contaminations can be systematically and recursively removed by using Richardson extrapolation or polynomial fitting. These aspects have been recently reviewed [19, 20]. The FF approach has been employed to calculate the static HRS response, β_{HRS}, of five reference molecules, CCl_4, $CHCl_3$, CH_2Cl_2, CCl_3CN, and CH_3CN [14]. Results sketched in Fig. 6.2 show that electron correlation effects might be quite different as a function of the chemical nature. Considering the CCSD(T) results as the reference, general—but not systematic—trends are observed. First, the HF values generally underestimate the CCSD(T) results, up to 50% in the case of CH_3CN. An improvement is achieved by using the second-order Møller–Plesset (MP2) perturbation theory method so that the MP2 values underestimate or overestimate the CCSD(T) values by up to 20–25%. Finally, missing the perturbative triples, the β_{HRS} responses are underestimated by up to 15% for CCl_4 and CCl_3CN, whereas the difference with respect to CCSD(T) is much smaller for compounds with fewer chlorine atoms (less than 1% and 6% for CH_3CN and CH_2Cl_2, respectively).

Alternatively, β can be calculated by employing response function approaches [21, 22], which are equivalent to evaluate analytically the responses of the dipole moment to external fields oscillating at finite frequencies. At the HF level, this approach gives rise to the time-dependent HF (TDHF) method [23]. Within the density functional theory (DFT) formalism, it gives the time-dependent DFT (TDDFT) scheme [24]. A hierarchy of coupled-cluster (CC) models has also been

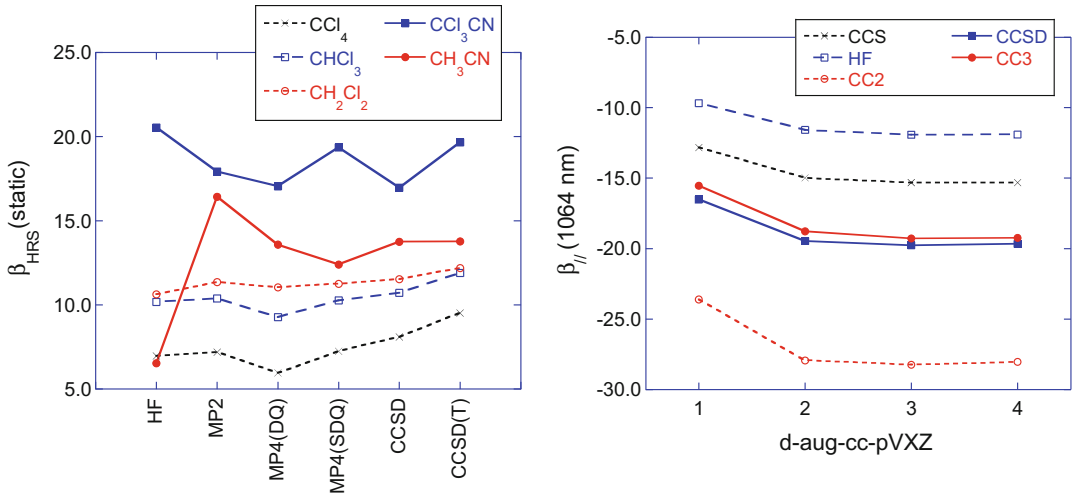

Fig. 6.2 Basis set and electron correlation effects on β (a.u.). *Left* static β_{HRS} of five reference molecules evaluated with the d-aug-cc-pVTZ basis set; *right* dynamic $\beta_{//}(-2\omega;\omega,\omega)$ ($\lambda = 1064$ nm) of water

elaborated: CCS=CIS, CC2, CCSD, and CC3, which allows controlling the convergence of the responses as a function of the level of treatment of electron correlation [22]. Figure 6.2 illustrates the convergence of the EFISHG response, $\beta_{//}$, of water as a function of the basis set and of the level of electron correlation. Like in Fig. 6.1, the convergence with basis set size is smooth, though it is faster at the HF and CCS level than when using higher-order methods. Then, for a given basis set, the ordering of the $\beta_{//}$ amplitudes according to the method is:

$$\text{HF} < \text{CCS} < \text{CC3} \approx \text{CCSD} < \text{CC2} \tag{6.5}$$

Again, the contribution from the triples, as estimated from the difference between the CCSD and CC3 results, is small. On the other hand, the CC2 method overestimates $\beta_{//}$ by as much as 50%, whereas the $\beta_{//}$ amplitude is strongly underestimated at the HF (40%) and CCS (20%) levels of approximation. For the CC levels, the $\beta_{//}$ amplitude ordering follows the relative values of the lowest excitation energies, dominating the β response [25] (in the case of the $^1A_1$ state, the vertical excitation energies calculated with the d-aug-cc-pVTZ basis set amount to 10.79 eV (HF), 10.81 eV (CCS), 9.82 eV (CC3), 9.81 eV (CCSD), and 9.59 eV (CC2)).

Still, frequency-dependent hyperpolarizabilities evaluated at high-order electron correlation levels are not always available, so that various approximate schemes have been proposed. They combine static correlated values with static and dynamic responses evaluated at lower levels of approximation. A multiplicative or percentage approximation (MA) has been proposed by Sekino and Bartlett [26], and an additive approximation (AA) by Rice and Handy [27]:

$$^{MA}\beta_{HRS}^{CCSD}(\omega) = \beta_{HRS}^{CCSD}(0) \times \frac{\beta_{HRS}^{HF/DFT}(\omega)}{\beta_{HRS}^{HF/DFT}(0)} \tag{6.6}$$

$$^{AA}\beta_{HRS}^{CCSD}(\omega) = \beta_{HRS}^{CCSD}(0) + \left[\beta_{HRS}^{HF/DFT}(\omega) - \beta_{HRS}^{HF/DFT}(0)\right] \tag{6.7}$$

Besides their widespread use, these approximations have been assessed in a limited number of studies [28 and references therein]. In the case of CCl_4, both MA and AA based on HF frequency dispersions underestimate β_{HRS} ($\lambda = 632$ nm) by about 20%, whereas for CH_2Cl_2, the underestimation is smaller with MA (8%) than AA (12%). More drastically, the effect of the frequency dispersion of CCl_4 is qualitatively wrong when adopting the HF method, since it suggests a decrease of β_{HRS} with the photon energy (Fig. 6.3), whereas CCSD calculations predict an increase of its amplitude. A much less frequently used alternative consists in describing frequency dispersion at the TDDFT level. So, LC-BLYP and B3LYP behave better than HF for the CCl_4 molecule with an increase of β_{HRS} with the frequency, though slightly slower than with CCSD. Similarly, for CH_2Cl_2, LC-BLYP (B3LYP) closely reproduces the CCSD frequency dispersion with small overestimations (underestimations). M06 (data not shown) and BLYP frequency dispersions are also close to the CCSD reference for CH_2Cl_2, whereas for CCl_4, M06 overestimates it substantially. These differences of frequency dispersion can be related to the relative values of the excitation energies (smaller with B3LYP than with CCSD), as well as of the transition dipoles, and excitation-induced dipole moment variations.

Comparisons of the CC3/d-aug-cc-pVQZ $\beta_{//}$ values of H_2O (−19.28 and −21.77 a.u. at 1064 and 694.3 nm, respectively) with experimental values (−19.2 ± 0.9 [29] and −22/0 ± 0.9 a.u. [30]) substantiate the predictability of the method and confirm the small amplitude of the vibrational contributions (note that the pure vibrational and zero-point vibrational average contributions might also be

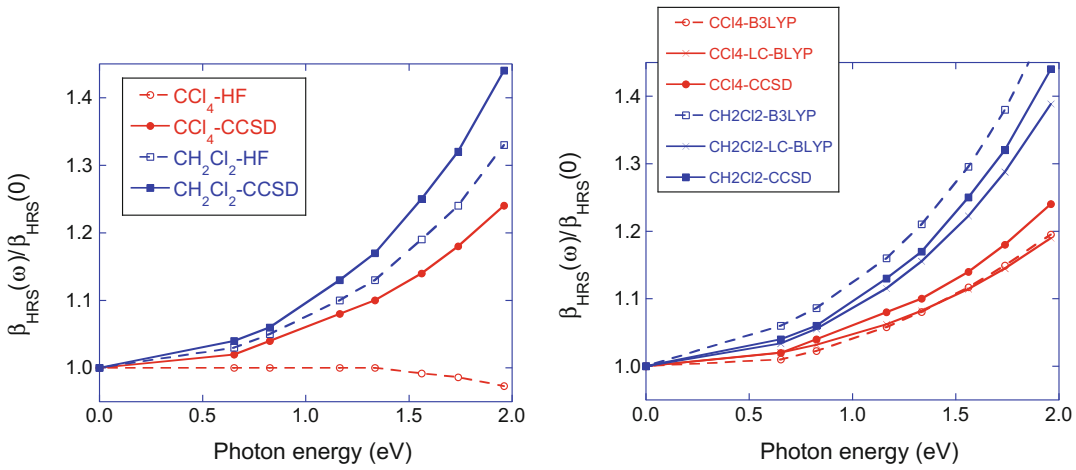

Fig. 6.3 Frequency dispersion on β_{HRS} described at the TDHF (*left*) or TDDFT (*right*) levels of approximation in comparison with CCSD, as determined with the d-aug-cc-pVDZ basis set

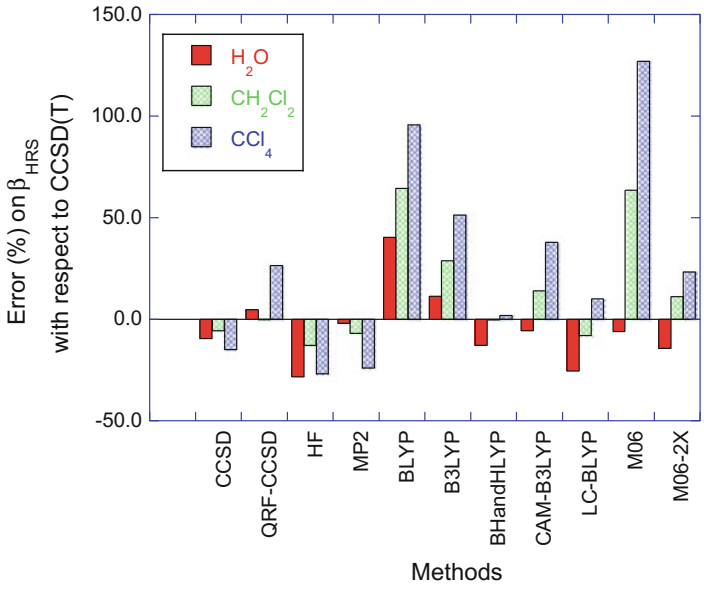

Fig. 6.4 Error (%) on the static β_{HRS} of H_2O, CH_2Cl_2, and CCl_4 for different exchange-correlation functionals and levels of approximation in comparison with CCSD(T). The calculations were performed with the d-aug-cc-pVTZ basis set. MP2, CCSD, and CCSD (T) results were obtained from the FF calculations, the QRF-CCSD calculations using the response method, and the HF and DFT calculations with the coupled-perturbed analytical differentiation procedures

non-negligible while canceling each other). In the case of CCl_4, Shelton [31] reported an experimental β_{HRS} (at 1064 nm) value of 12.8 ± 1.1 a.u. in comparison with a theoretical estimate of 14.3 a.u. The latter value was obtained by adding to the electronic dynamic CCSD value (14.9 a.u.) [28], the ZPVA (−1.1 a.u.), and pure vibrational (0.5 a.u.) contributions of [32].

Though small systems such as H_2O, CCl_4, and CH_2Cl_2 allow using computationally demanding techniques and therefore tackling the convergence of the molecular properties as a function of electron correlation level, it is worth assessing the reliability of more approximate schemes in view of applying these to larger systems. In particular, there is an interest to assess the performance of density functional theory (DFT) with conventional as well as with most recent exchange-correlation functionals in comparison with the Hartree–Fock method and to MP2. Following Ref. [33], different levels of approximation have been assessed in comparison with FF CCSD(T) calculations (Fig. 6.4). Systematic trends are observed: (i) BLYP overestimates β_{HRS} by as much as 100% for CCl_4; (ii) this overestimation decreases when adding 20% of HF exchange (B3LYP) but not for CH_2Cl_2 and CCl_4 with M06 (28% HF exchange) so that with these three functionals the accuracy is lower than with HF, which underestimates β_{HRS} by 15–30%; (iii) then, further increasing the percentage of HF exchange (BHandHLYP (50%) and M06-2X (56%)) leads to improvements; and (iv) finally, range-separated hybrids perform also better, but the improvement is not systematic (CAM-B3LYP reproduces closely the response of H_2O, but the error on CCl_4 is as large as 40%, whereas with LC-BLYP, β_{HRS} of H_2O is underestimated by 25% and the responses of the two other compounds are close to CCSD(T)). On the other hand, Karamanis et al. [34] have shown that for doped Si clusters, hybrid GGA with 20–25% HF exchange performs better than hybrid GGAs with larger percentage of HF exchange or than long-range corrected hybrids. So, without considering push-pull π-conjugated systems for which the XC requirements are also function of their

size and charge-transfer character [35–39], the reliability of DFT depends strongly on the XC functional and there is no easy clue to select a priori an accurate XC functional. Still, the best functionals are global or range-separated hybrids and include substantial amounts of HF exchange.

When using DFT approaches, an additional parameter to control is the density of the integration grid. The Gaussian09 grids are called `Fine`, `UltraFine`, and `SuperFine`, and they differ by the number of radial shells (75, 99, and 150, respectively) and of angular points per shell (302, 590, and 974). In a recent investigation [33], it was found that for TDDFT calculations of small reference molecules, the β_{HRS} differences could attain up to 1 a.u. (up to 5%) between the UltraFine and SuperFine grids when employing meta-GGA XC functionals, whereas this difference is only of ~0.02 a.u. when using GGA or hybrid XC functionals. In fact, the situation is even more complex when considering that β tensor components can be evaluated from the FF approach as the first-, second-, and third-order derivatives. Let us consider the β_{zxx} component:

$$\beta_{zxx} = -\left(\frac{\partial^3 E}{\partial E_z \partial E_x^2}\right)_0 = \left(\frac{\partial^2 \mu_z}{\partial E_x^2}\right)_0 = \left(\frac{\partial \alpha_{zx}}{\partial E_x}\right)_0 \tag{6.8}$$

For variational wave functions, these three quantities are expected to be identical and also identical to the fully analytical TDDFT/CPKS value. We have performed such FF calculations for β_{zxx} of H_2O. A selection of Romberg's tables is provided in Table 6.1. In these calculations, the threshold on the energy has been lowered to 10^{-11} a.u. As discussed in the previous works [19, 20], each table presents the same structure. In particular, for n = 0, by going from k = 0 to k = 6, the β values vary randomly until a given k value where β starts increasing monotonically. At smaller k's, these variations originate from the lack of precision on the field-dependent properties (α, μ, or E). At larger k's, the monotonic behavior results from the higher-order contaminations, which can then be iteratively and systematically removed using Romberg's quadrature. This allows locating stability domains for β and therefore converged β values. Considering β as the first-order derivative of α, a converged value of 3.37 a.u. is obtained using a `Fine` grid. An `UltraFine` grid (as well as a `SuperFine` grid, results not shown) gives a value of 3.36 a.u. Analyzing the variations of β_{zxx} as a function of the order of Romberg's iteration *(n)* and of the field amplitude *(k)* tells that the numerical accuracy on β_{zxx} is of the order of 0.01 a.u., consistently with an accuracy of 10^{-4} a.u. on the field-dependent polarizabilities. This value of 10^{-4} is obtained by taking the product between the accuracy on β_{zxx} and the field amplitude for $k = 4$, which corresponds to the smallest field amplitude associated with the converged value. A similar accuracy is achieved by considering the second-order derivative of μ with non-negligible differences in the Romberg's tables when going from the `UltraFine` to the `SuperFine` grid and large differences between the `Fine` and `UltraFine` grids. This highlights a reduction of accuracy on the dipole moment values. Moreover, these data are consistent with an accuracy of about 10^{-6} a.u. on the field-dependent dipole moments.

Table 6.1 Romberg's table for the evaluation of β_{zxx} of H_2O as a function of the order of the derivative and the quality of the integration grid. The LC-BLYP XC functional was employed together with the aug-cc-pVTZ basis set. *n* represents the number of Romberg's iterations, where higher-order contaminations are removed. *k* determines the field amplitude, $E = E_0\ 2^k$ with $E_0 = 0.0004$ a.u. Best/converged values are indicated by an arrow

	n = 0	n = 1	n = 2	n = 3	n = 4	n = 5	n = 6
First-order derivative of α, grid = `Fine`							
k = 0	3.37314	3.37341	3.37376	3.37387	3.37390	3.37391	3.37391
k = 1	3.37234	3.36812	3.36688	3.36655	3.36647	3.36645	
k = 2	3.38499	3.38674	3.38730	3.38744	3.38747		
k = 3	3.37975	3.37835	3.37863	3.37871			
k = 4	3.38393	3.37414	3.37394		→	**3.37**	
k = 5	3.41329	3.37707					
k = 6	3.52197						
First-order derivative of α, grid = `UltraFine`							
k = 0	3.36461	3.36776	3.36869	3.36893	3.36899	3.36901	3.36901
k = 1	3.35517	3.35382	3.35355	3.35348	3.35346	3.35346	
k = 2	3.35922	3.35792	3.35777	3.35774	3.35773		
k = 3	3.36313	3.36009	3.35993	3.35989			
k = 4	3.37223	3.36257	3.36252		→	**3.36**	
k = 5	3.40122	3.36331					
k = 6	3.51496						
Second-order derivative of μ, grid = `Fine`							
k = 0	4.25000	4.47188	4.52941	4.54396	4.54761	4.54853	4.54875
k = 1	3.58437	3.60885	3.61255	3.61331	3.61349	3.61354	
k = 2	3.51094	3.55339	3.56461	3.56745	3.56816		
k = 3	3.38359	3.38504	3.38557	3.38570			
k = 4	3.37925	3.37708	3.37771		→	**3.38**	
k = 5	3.38577	3.36750					
k = 6	11.49397						
Second-order derivative of μ, grid = `UltraFine`							
k = 0	3.58750	3.63437	3.64684	3.65002	3.65082	3.65102	3.65107
k = 1	3.44688	3.44740	3.44630	3.44595	3.44585	3.44583	
k=2	3.44531	3.46387	3.46843	3.46956	3.46985		
k=3	3.38965	3.39538	3.39714	3.39758			
k=4	3.37246	3.36898	3.36928		→	**3.37**	
k=5	3.38290	3.36445					
k=6	3.43824						

(continued)

Table 6.1 (continued)

	n = 0	n = 1	n = 2	n = 3	n = 4	n = 5	n = 6
Second-order derivative of μ, grid = `SuperFine`							
k = 0	3.62500	3.63854	3.63778	3.63731	3.63718	3.63714	3.63713
k=1	3.58437	3.65000	3.66720	3.67156	3.67265	3.67292	
k=2	3.38750	3.39193	3.39301	3.39328	3.39334		
k=3	3.37422	3.37567	3.37631	3.37647			
k=4	3.36987	3.36603	3.36626		→	**3.37**	
k=5	3.38141	3.36261					
k=6	3.43781						
Third-order derivative of E, grid = `Fine`							
k = 0	3.34710	3.34181	3.34038	3.34001	3.33992	3.33990	3.33989
k = 1	3.36296	3.36329	3.36343	3.36347	3.36348	3.36348	
k = 2	3.36197	3.36121	3.36120	3.36119	3.36119		
k = 3	3.36424	3.36146	3.36147	3.36147	→	**3.361**	
k = 4	3.37256	3.36142	3.36135				
k = 5	3.40599	3.36251					
k = 6	3.53643						
Third-order derivative of E, grid = `UltraFine`							
k = 0	3.35632	3.35569	3.35560	3.35559	3.35558	3.35558	3.35558
k = 1	3.35820	3.35693	3.35664	3.35657	3.35655	3.35655	
k = 2	3.36201	3.36129	3.36128	3.36128	3.36128		
k = 3	3.36417	3.36135	3.36135	3.36135	→	**3.361**	
k = 4	3.37262	3.36146	3.36139				
k = 5	3.40608	3.36259					
k = 6	3.53655						

Finally, the best accuracy is achieved by considering the third-order derivative of the energy, leading to a value of 3.361 a.u. (if not 3.3613 a.u.). Using an `UltraFine` grid provides slightly more accurate results than the `Fine` grid, whereas there is almost no difference with the `SuperFine` grid. Further calculations were performed with a (very tight) threshold of 10^{-13} a.u. on the energy, which is not going to work for any compound and the whole set of field amplitudes, and they did not lead to improvements. So, to get highly accurate results, a `Fine` grid can be used but in combination with third-order energy derivatives, whereas the `UltraFine` grid is recommended together with first-(second-)order derivatives of α (μ) because the number of significant digits on the energy is larger than on μ and on the CPKS α.

6.3 Small Molecules in Solution

Implicit solvation models like the polarizable continuum model (PCM) [40] are usually employed to account for the effects of solvation on the first hyperpolarizability. These models describe the solvent as a structureless polarizable continuum

characterized by, among other parameters, its macroscopic dielectric permittivity, which depends on the frequency of the applied field. For CCl_4, the dielectric constant or relative permittivity amounts to 2.23 (ε_0) and 2.13 (ε_∞) in the zero (static) and infinite frequency limit, respectively. On the other hand, for CH_2Cl_2, the difference is much larger with $\varepsilon_0 = 8.93$ and $\varepsilon_\infty = 2.03$, owing to the orientation contribution related to the dipolar character of dichloromethane. This impacts directly the β responses, which are enhanced by the self-consistent reaction field. So, at the HF/d-aug-cc-pVTZ level, the $\beta_{HRS,LIQ}/\beta_{HRS,GAS}$ ratio of CCl_4 amounts to 1.43 and 1.39 for infinite and 1064 nm wavelengths, respectively, whereas for the dipolar CH_2Cl_2, it goes from 2.39 to 1.78 [14]. Then, accounting for electron correlation effects is not straightforward if the calculations are performed with the FF method, i.e., at zero frequency. Indeed, for dipolar solvents, the static dielectric constant is larger than the dynamic ones, which will lead to overestimations of the solvent effects and of the β amplitudes. A practical issue would be to use an effective static dielectric constant that only accounts for polarization contributions, neglecting the orientational contributions of the solvent. Another approach consists in correcting these static responses by including frequency dispersion with Eqs. 6.6 and 6.7:

$$^{MA}\beta_{HRS}^{CCSD,PCM}(\omega) = \beta_{HRS}^{CCSD,PCM}(0) \times \frac{\beta_{HRS}^{HF/DFT,PCM}(\omega)}{\beta_{HRS}^{HF/DFT,PCM}(0)} \tag{6.9}$$

$$^{AA}\beta_{HRS}^{CCSD,PCM}(\omega) = \beta_{HRS}^{CCSD,PCM}(0) + \left[\beta_{HRS}^{HF/DFT,PCM}(\omega) - \beta_{HRS}^{HF/DFT,PCM}(0)\right] \tag{6.10}$$

In this case, all the properties (the high-level static response as well as the static and dynamic TDHF or TDDFT responses) are performed using implicit solvation models. Consequently, two static β calculations are performed and their overestimations cancel each other, though incompletely. On the other hand, combining frequency dispersion as obtained from the two-state approximation [41] with high-level static PCM results will not be appropriate, besides in cases where an effective static dielectric constant is used.

Table 6.2 presents HRS quantities calculated for five reference molecules at the CCSD(T) level in combination with the MA scheme: β_{HRS}, the depolarization ratio (DR), which is determined by the shape of the NLOphore, the dipolar ($|\beta_{J=1}|$) and octupolar ($|\beta_{J=3}|$) components, and their ratio, the nonlinear anisotropy parameter, $\rho = |\beta_{J=3}|/|\beta_{J=1}|$. They are compared to the experimental values [14]. For all compounds, the octupolar character is overestimated although the experimental ordering of the DR (and ρ) is reproduced. Additional calculations not reported here show that this hierarchy of DR is already reproduced at the HF level, but the underestimation of the DR values is more severe than at the CCSD(T) level. Then, considering that the standard deviations on the experimental values is typically of 10%, most of the calculated β_{HRS} values match the experimental ones, in particular for $CHCl_3$ and CCl_3-CN, but also for CH_2Cl_2 and CH_3-CN, with errors smaller than 25%. On the other hand, for CCl_4, the underestimation is substantial and attains 50%. A large part of this underestimation originates from the HF frequency dispersion that is

Table 6.2 Dynamic ($\lambda = 1064$ nm) β_{HRS}, DR, $|\beta_{J=1}|$, $|\beta_{J=3}|$, and ρ values (a.u.) as determined at the CCSD(T)/d-aug-cc-pVTZ level of approximation using the MA scheme (Eq. 6.6) and accounting for solvent effects with the PCM approach in its Integral Equation Formalism (IEF) in comparison with experiment [14]. Values in parentheses are the differences (%) with respect to the experimental values (for β_{HRS}) or the experimental values (DR and ρ)

	CCl_4	$CHCl_3$	CH_2Cl_2	CCl_3–CN	CH_3–CN
β_{HRS}	13.73 (−53)	19.74 (+4)	23.14 (+16)	22.41 (−10)	40.48 (23)
DR	1.50 (1.50)	1.90 (2.61 ± 0.02)	3.36 (4.21 ± 0.03)	2.16 (2.98 ± 0.03)	6.80 (8.40 ± 0.15)
$\|\beta_{J=1}\|$	0.00	17.89	37.02	25.10	81.77
$\|\beta_{J=3}\|$	44.49	57.82	49.24	61.66	40.07
ρ	∞ (∞)	3.22 (1.84 ± 0.02)	1.33 (1.01 ± 0.01)	2.46 (1.54 ± 0.02)	0.49 (0.23 ± 0.15)

combined with CCSD(T) static responses [14] and, when describing frequency dispersion at the CCSD level as discussed in Sect. 2, the error is reduced by a factor of 2 [28]. These successive studies demonstrate that there is an interest in performing high-level calculations with explicit solvent molecules as well as in reassessing the amplitude of the vibrational contributions, the pure vibrational contribution that is usually negligible for the second harmonic generation and the zero-point vibrational average. In particular, the non-polar but highly polarizable CCl_4 molecule appears to be a challenging case.

Still, for CCl_4, these comparisons between experiment and theory assumed that each molecule behaves like an independent light scatterer, giving rise to the so-called incoherent HRS signal, which is purely octupolar. Nevertheless, Kaatz and Shelton [42] have shown that the experimental HRS signal contains both a coherent (β_{coh}) and an incoherent (β_{incoh}) part, with $\beta_{coh}/\beta_{incoh} \sim 2/3$. This coherent response originates from the interactions between the CCl_4 molecules and attributes to liquid CCl_4 both dipolar ($|\beta_{J=1}|$) and octupolar ($|\beta_{J=3}|$) HRS responses. The description of the dual contribution to β_{HRS} of liquid CCl_4 has been challenged by sequential QMMM calculations. The method consists first in performing Monte Carlo simulations to generate uncorrelated snapshots representing the liquid structure [43, 44] and then in calculating at the QM level the first hyperpolarizability for a selection of these snapshots [45]. In these QM calculations, the solvent (surrounding molecules) is described either exclusively by point charges or by considering explicitly a few neighboring CCl_4 molecules, embedded in point charges of the remaining solvent molecules. It has been observed that considering explicitly a few neighboring CCl_4 molecules embedded in point charges enables monitoring the emergence of the dipolar contribution to $\beta_{HRS,LIQ}$, characterized by an increase of DR and a decrease of ρ. So, combining the Hartree–Fock method and the aug-cc-pVQZ basis set for feasibility purpose, with two interacting CCl_4 molecules, DR attains 2.34 ± 0.66 ($\rho = 2.11$) while when considering five interacting molecules $DR = 2.78 \pm 0.92$ ($\rho = 1.81$) [46]. Figure 6.5 illustrates the convergence of β_{HRS} as a function of the number of snapshots in the case of five interacting molecules embedded in point charges. Note that the amplitude of β_{HRS} per CCl_4 molecule is little impacted when accounting for these specific intermolecular interactions. These calculations have confirmed to a large extent the experimental data and have substantiated that the dipolar contribution originates from intermolecular interactions between the CCl_4 molecules. Nevertheless, it remains challenging to perform high-level ab initio calculations on such CCl_4 clusters, which expectedly will modify the description of the intermolecular interactions and their impact on β_{HRS}, because calculating the first hyperpolarizability of CCl_4 requires using an extended basis set with diffuse functions.

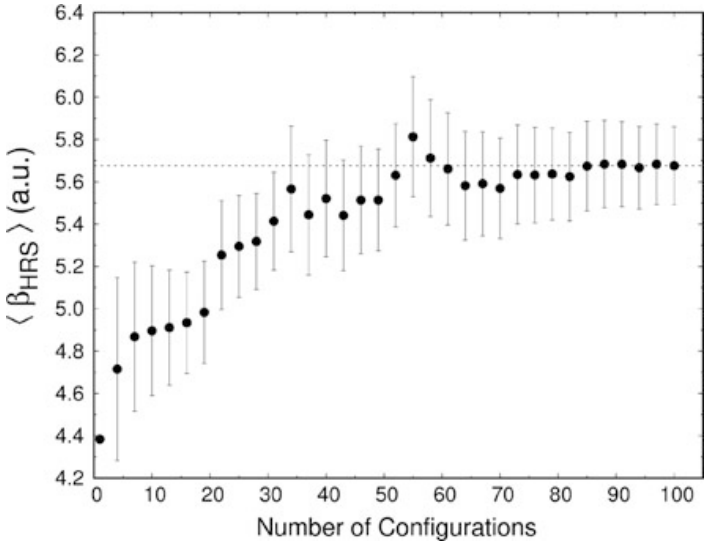

Fig. 6.5 Statistical convergence of β_{HRS} per CCl_4 molecule calculated at the HF/aug-cc-pVQZ level as a function of the number of configurations (snapshots). Each calculation was performed for a cluster of five molecules of CCl_4 solvated by point charge embedding. The *horizontal line* gives the averaged value and the uncertainty corresponds to the statistical error

6.4 Extended π-Conjugated Dyes

Basis set effects on the first hyperpolarizability of a π-conjugated dye were assessed in the case of an oxazine derivative (Scheme 6.1), which can switch between a closed and an open form upon triggering with light irradiation, as well as with pH and redox potential variations [47]. The calculations were performed at the TDHF level ($\lambda = 1064$ nm) on the closed form, which presents a rather small β_{HRS} response, and on the zwitterionic open form, whose β_{HRS} is enhanced due to push-pull electron delocalization effects. Solvent effects were accounted for by using the IEFPCM scheme [40]. Table 6.3 reports the β_{HRS} values of the two forms, their contrasts, β_{HRS}(open)/β_{HRS}(closed), and the corresponding depolarization ratios. In the case of the closed form, starting from the 6-31G(d) basis set, adding *p* polarization functions on the H atoms has a negligible impact on β_{HRS}. On the other hand, adding a set of *sp* diffuse functions leads to an increase of β_{HRS} by 20% while the addition of a second set of diffuse functions does not change significantly the β_{HRS} values. Note that starting from the Dunning cc-pVDZ basis set, β_{HRS} is 6% smaller than with the 6-31G(d) basis while going to cc-pVTZ, cc-pVQZ, and cc-pV5Z leads to increases of 1%, 8%, and 13% with respect to 6-31G(d), respectively. However, these basis sets contain much more contracted GTOs than 6-31G(d). The 6-31G (and, to a lower extent, 6-311G) β_{HRS} value is also larger than the 6-31G(d) one, indicating that the inclusion of polarization and diffuse functions has counteracting effects. Finally, the values obtained with the aug-cc-pVDZ and aug-cc-pVTZ basis sets are in close agreement with those of the Pople basis set series, provided at least one set of diffuse functions is included.

The basis set effects are even smaller in the case of the oxazine open form. Indeed, going from 6-31G(d) to 6-31+G(d), β_{HRS} increases only by 12% while from 6-31G(d) to 6-31G β_{HRS} increases by 3%. Then, the differences with respect to 6-31G(d) amounts to –2%, 1%, 4%, and 6% for cc-pVDZ, cc-pVTZ, cc-pVQZ, and

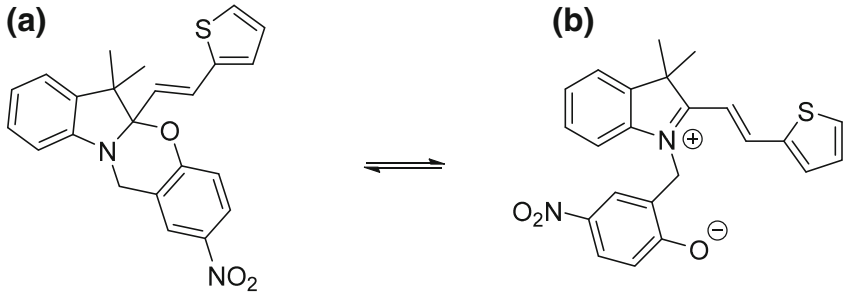

Scheme 6.1 Closed (*left*) and open (*right*) forms of an oxazine derivative. Switching from the closed to open form can be triggered by light irradiation to form a zwitterion or by decreasing the pH to get the corresponding protonated cationic species [47]

Table 6.3 Effect of the basis set on the HRS first hyperpolarizability (β_{HRS}) and its depolarization ratio (in parentheses) of the closed (**a**) and open (**b**) forms of an oxazine derivative as well as on the β_{HRS} contrast ratio, β_{HRS}(open)/β_{HRS}(closed). The calculations were performed at the TDHF level with a wavelength of 1064 nm, while solvent (acetonitrile) effects were included using the IEFPCM scheme. The numbers in parentheses in the first column correspond to the number of contracted GTOs

	β_{HRS}(closed)	β_{HRS}(open)	β_{HRS}(open)/β_{HRS}(closed)
6-31G (305)	841 (4.00)	3939 (5.94)	4.75
6-311G (445)	816 (3.89)	4019 (5.92)	4.92
6-31G(d) (479)	748 (4.11)	3824 (5.81)	5.12
6-31G(d,p) (539)	749 (4.11)	3830 (5.80)	5.11
6-311G(d) (590)	742 (4.00)	3903 (5.80)	5.26
6-31+G(d) (590)	895 (3.93)	4299 (5.92)	4.80
6-31++G(d) (615)	891 (3.90)	4290 (5.92)	4.81
6-311+G(d) (699)	914 (3.94)	4292 (5.95)	4.70
6-311+G(d,p) (759)	915 (3.93)	4298 (5.94)	4.70
6-311++G(d) (717)	910 (3.92)	4286 (5.95)	4.71
cc-pVDZ (510)	701 (3.96)	3748 (5.78)	5.34
cc-pVTZ (1154)	755 (3.94)	3880 (5.85)	5.14
cc-pVQZ (2199)	809 (3.97)	3984 (5.90)	4.92
cc-pV5Z (3743)	849 (4.00)	4057 (5.92)	4.77
aug-cc-pVDZ (848)	902 (4.00)	4194 (5.96)	4.65
aug-cc-pVTZ (1798)	897 (4.01)	4135 (5.95)	4.61

cc-pV5Z, respectively. Similarly, the aug-cc-pVDZ β_{HRS} value is only 2% smaller than the 6-31+G(d) value. Finally, the calculations performed with the aug-cc-pVTZ basis set, which, among those employed here, should be considered as the most flexible basis set for calculating the first hyperpolarizability, give β_{HRS} values slightly smaller than those obtained with the aug-cc-pVDZ (–1%), 6-31+G (d) (–4%), 6-31++G(d) (–4%), 6-311+G(d) (–4%), and 6-311++G(d) (–4%) basis sets.

The combined effect of basis set extension on the first hyperpolarizability of the closed and open form results therefore in a slight decrease of the β_{HRS}(open)/β_{HRS}(closed) contrast ratio, from 5.12 with 6-31G(d) to 4.71, 4.65, and 4.61 with the 6-311++G(d), aug-cc-pVDZ, and aug-cc-pVTZ basis sets, respectively. Again, the 6-31G value is very close to the result obtained with the largest basis set. The effect of the basis set size on the depolarization ratio of both forms is also very weak, demonstrating that the dipolar versus octupolar contributions to β_{HRS} are already estimated within ±3% with the 6-31G(d) basis set. Still, increasing the basis set size decreases DR of the closed form (i.e., leads to a relative increase of the octupolar contribution), whereas for the open form, it leads to an increase of DR, or of the dipolar contribution to β_{HRS}.

Consequently, in agreement with other studies [36], the requirements on the basis set are much less stringent for estimating β_{HRS} and DR of a π-conjugated push-pull molecule than for a small molecule.

Electron correlation effects have then been analyzed in the case of *p*-nitroaniline, using the aug-cc-pVDZ basis set. Static β values have been obtained using the FF approach (Table 6.4). The same B3LYP/6-311G(d) geometry was used for all β calculations. Using the CCSD(T) results as references, the HF methodology strongly underestimates both β_{HRS} and $\beta_{//}$ but most of the error is recovered by including electron correlation at the second order (MP2). Then, higher-order corrections have detrimental or canceling contributions to β. Note that the inclusion of the triples (MP4 vs. MP4SDQ and CCSD vs. CCSD(T)) amounts to a correction of

Table 6.4 HRS and EFISHG first hyperpolarizabilities (β_{HRS} and $\beta_{//}$) (in a.u.) and HRS depolarization ratios (DR) of *p*-nitroaniline as determined at different levels of approximation with the aug-cc-pVDZ basis set. All values have been obtained using the FF approach and are compared to the reference results obtained at the Ref = CCSD(T) level

	β_{HRS} (DR)	β_{HRS}(X)/β_{HRS}(Ref)	$\beta_{//}$	$\beta_{//}$(X)/$\beta_{//}$(Ref)
HF	397.8 (3.23)	0.586	479.4	0.516
MP2	668.4 (4.36)	0.985	919.0	0.989
MP3	579.8 (4.03)	0.855	774.3	0.883
MP4D	621.4 (4.18)	0.916	841.2	0.905
MP4DQ	551.1 (4.01)	0.812	734.0	0.790
MP4SDQ	577.9 (4.09)	0.852	776.3	0.835
MP4	648.7 (4.28)	0.956	886.2	0.953
CCSD	607.6 (4.14)	0.896	819.6	0.882
CCSD(T)	**678.4 (4.31)**	**1.000**	**929.4**	**1.000**
BLYP	749.2 (4.03)	1.104	1001.7	1.078
B3LYP	686.9 (4.00)	1.012	915.8	0.985
BHandHLYP	567.4 (3.83)	0.836	742.8	0.799
M06	622.7 (3.89)	0.918	820.4	0.883
M06-2X	551.3 (3.87)	0.813	724.8	0.780
CAM-B3LYP	598.7 (3.95)	0.883	793.6	0.854
LC-BLYP	527.6 (3.90)	0.778	695.7	0.749

about 10%. The variations of DR are smaller but follow the same trends as those of β_{HRS}, demonstrating that the inclusion of electron correlation mostly increases the dipolar component of β_{HRS}.

Using DFT and conventional XC functionals, the results get more contrasted. BLYP overestimates the β values (but not DR) by about 10%. Then, adding larger and larger amounts of HF exchange in the functional lead to a reduction of β_{HRS} and $\beta_{//}$ so that the agreement is excellent between B3LYP (20% HF exchange) and CCSD(T), whereas the BHandHLYP (50% HF exchange) values are underestimated. Similar effects are observed between M06 (27% HF exchange) and M06-2X (54% HF exchange), where for the later the underestimations attain 20%, similar to what is found for BHandHLYP. The use of range-separated hybrids follows also the same trend with the smallest values obtained with the LC-BLYP functional (underestimations of 22 and 25%) and then CAM-B3LYP (underestimations of 12 and 15%). Indeed, at long range ($r \rightarrow \infty$) LC-BLYP includes 100% of HF exchange, whereas CAM-B3LYP only 65%.

These results need however to be completed by those on other push-pull π-conjugated systems, with π-conjugated segments of different lengths and D/A groups of different strengths. In the case of α,ω-nitro, dimethylamino-polyenes containing 4 and 6 CH=CH units, the β(HF)/β(MP2) ratio amounts to 0.411 and 0.419, respectively [28]. Though these ratios have been obtained for the dominant longitudinal β tensor component with the 6-31+G(d) basis set, they can be compared with the $\beta_{//}$ ratio of 0.521 obtained here for *p*-nitroaniline. Similarly, the corresponding values for the α,ω-nitro, dimethylamino-polyynes with 4 and 6 C≡C units amount to 0.582 and 0.616, demonstrating that the β(HF)/β(MP2) ratio can vary by about 20% for π-conjugated segments commonly found in push-pull π-conjugated compounds. So, it is often recognized that the MP2/HF ratio for the static β values is close to 2 with a standard deviation of about 20%. Moreover, for those push-pull π-conjugated polyenes and polyynes containing 4 units, the β(MP2)/β(CCSD(T)) ratio amounts to 1.045 and 0.997 respectively, in comparison with a value of 0.989 for $\beta_{//}$ of *p*-nitroaniline, respectively. So, as substantiated by additional related investigations [48, 49], for these compounds the MP2 approach is often a good compromise between accuracy and computational needs, but it requires using approximate schemes, like Eqs. 6.9–6.10, to describe frequency dispersion [20]. Still, benchmark results (CC3, CCSD, CCSD(T) together with a decent atomic basis set) on push-pull π-conjugated systems with 20–50 C atoms would be of high interest.

Again, for systems different from (and usually larger than) *p*-nitroaniline, the selection of a reliable XC functional for evaluating β and its modifications upon chemical changes is a subtle issue, which was already addressed in depth in many studies [35–39, 48, 50]. For medium-size compounds, the range-separated LC-BLYP hybrid functional has been shown to be reliable when characterizing the changes of β upon enlarging the π-conjugated linker from 4 to 6 CH=CH (or C≡C) units or upon changing the polyyne linker into a polyene segment [36]. On the other hand, the BLYP, B3LYP, and BHandHLYP functionals—as well as functionals with similar characteristics—generally perform quantitatively better, but the above chemical/size trends are poorly described. For instance, using the

6-31G(d) basis set, the β(B3LYP)/β(CCSD(T)) ratio amounts to 0.648 and 0.714 for the substituted polyenes with N = 4 and 6 (NMe_2-$(CH{=}CH)_N$-NO_2) but to 0.999 and 1.372 for their polyyne analogs (NMe_2-$(C{\equiv}C)_N$-NO_2), respectively [36]. Then, going toward even larger oligomers, the unphysical delocalization inherent to conventional (LDA, GGA, meta-GGA, and global hybrids) XC functionals gives rise to overestimations of the hyperpolarizabilities by more than one order of magnitude. This can be corrected by enforcing an asymptotically correct exchange-correlation potential, i.e., 100% of Hartree–Fock exchange. Still, as shown by early works [50], global hybrids with 100% HF exchange merely reproduce the β values calculated at the Hartree–Fock level. On the other hand, range-separated or long-range corrected (LC) hybrids, where the percentage of HF exchange varies with the inter-electronic distance, bring an improvement. This is evidenced by the β results of Kamiya et al. [48] on α,ω-nitro, amino-polyenes, where the LC-BOP results are larger than the HF ones, though smaller than the MP2 values. A further refinement of the XC functional consists in adjusting the range-separated parameter (μ) such that Koopmans' theorem is obeyed as closely as possible [51]. It is found that the optimal μ values are smaller than those recommended as standard values (0.30, 0.33 or 0.47 $bohr^{-1}$) and that they increase as a function of the size of the π-conjugated segment. So, in the case of (E)-N, N-dimethyl-4-(4-nitrostyryl)aniline derivatives containing from N = 1 to 4 CH=CH units between the phenyl rings, the LC-PBE and LC-PBE0 functionals with the standard μ = 0.30 value underestimate the MP2 β values for N = 3–4 by 18% and 27%, whereas using the optimal μ value, the corresponding functionals overestimate β by 15–24% and 12–21%, respectively [38]. For these systems, using the optimal μ value does not represent a clear improvement, whereas these optimally tuned range-separated hybrids perform clearly better than the conventional ones for N = 1–2. The complexity of selecting an appropriate XC functional has been further evidenced in a recent work due to Isborn and co-workers [39], recommending a larger fraction of exact exchange when computing β than for computing excitation energies. Thus, it is not clear whether exchange hybrid functionals could be further optimized to qualitatively and quantitatively reproduce MP2–or CCSD (T)–β values of increasingly large push-pull π-conjugated systems or, in other words, whether non-local exchange is sufficient in the absence of non-local correlation. Indeed, double hybrids, which include a given percentage of MP2 correlation, can provide for medium-size push-pull π-conjugated systems β values of at least similar quality as the global hybrids. Therefore, combining the same optimally tuned range-separated strategy for both HF exchange and MP2 correlation might lead to a functional for accurate prediction of β. Note however that the inclusion of MP2 correlation should be accompanied with an improvement over MP2 because the contrary would simply substantiate the use of MP2 to approximate CCSD(T).

Finally, the selection of an appropriate XC functional can also be addressed in the case of NLO switches (Scheme 6.2), molecules characterized by their ability to alternate between two or more chemical forms displaying contrasts in one of their NLO properties (here, the second harmonic intensity) [52]. In this case, besides the absolute values, their contrast is also of interest. Scheme 6.2 gives the structure of a

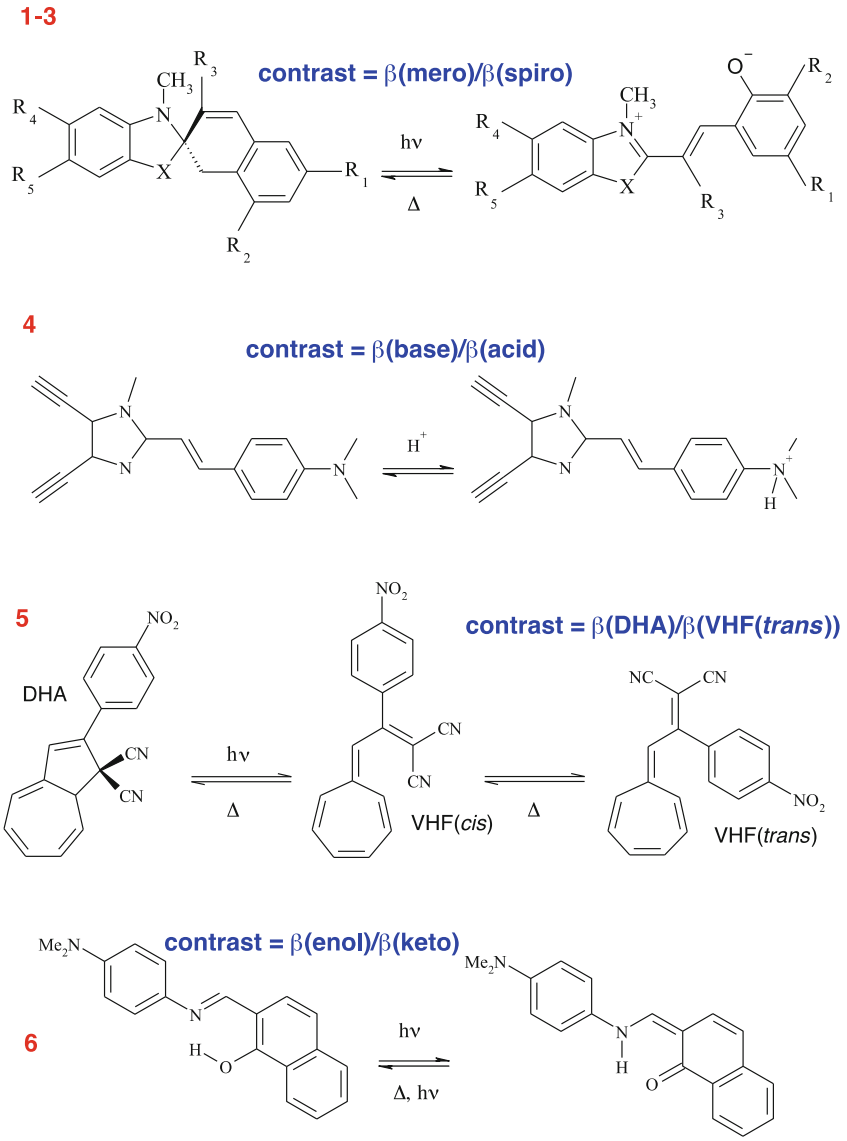

Scheme 6.2 Second-order NLO switches; **1–3** merocyanine–spiropyran with different combinations of substituents [**1**: R_1=NO_2, R_2=OMe, R_3=Me, X=S, R_4=R_5=H; **2**: R_1=NO_2, R_2=NMe_2, R_3=NH_2, X=NMe, R_4=H, R_5=NO_2; **3**: R_1=NO_2, R_2=NMe_2, R_3=NH_2, X=NMe, R_4=H, R_5=NO_2] [53]; **4** neutral and protonated forms of a 4,5-dicyanoimidazole derivative [54]; **5** dihydroazulene (DHA)-vinylheptafulvene (VHF) [55]; **6** tautomeric equilibrium of the N-(2-hydroxynaphtylidene) aniline [56]

selection of NLO switches that have recently been studied [53–56] as well as the targeted contrast. The reported calculations were carried out using the 6-311+G(d) basis set. The same geometries were used for the whole set of β calculations. Some of these calculations were already reported in Refs. [52, 57]. These correspond to static β_{HRS} values obtained in gas phase, except for compounds **6** where solvent (ethanol) effects were accounted for using the IEFPCM scheme. The results are shown in Fig. 6.6. Again, there are large variations of β amplitudes among the different methods. Considering that the MP2 method provides reference values to

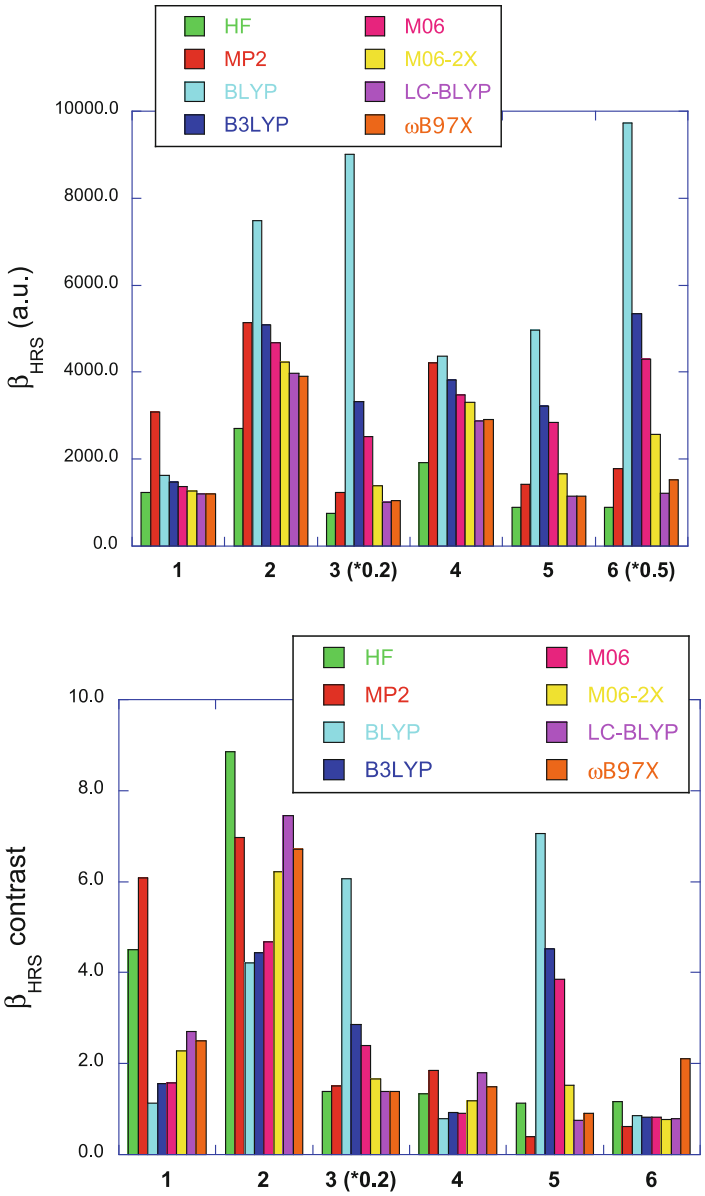

Fig. 6.6 Comparisons between HF, MP2, and DFT with different XC functionals to evaluate the static β_{HRS} of molecular switches. (top) β_{HRS} of chromophores **1**–**6** in one of their forms (merocyanine form for **1**–**3**; base form for **4**, DHA form for **5**, and enol form for **6**) and (bottom) β_{HRS} contrasts. The "*0.2" and "*0.5" labels on the x-axis mean that the corresponding β_{HRS} or β_{HRS} contrast values have been multiplied by the corresponding factor, for a question of readability

assess the XC functionals, the trend that the BLYP XC functional overestimates the static β_{HRS} values of compounds **2**–**6** is confirmed (though for compound **4** the agreement is better) and is related to the lack of HF exchange. Then, adding a small percentage of HF exchange (B3LYP and M06) improves the results for compounds **2** and **4,** whereas large overestimations are still observed for **3**, **5**, and **6**. Moving from M06 to M06-2X leads to a further improvement for a third compound (**3**). Then, including long-range Hartree–Fock exchange (LC-BLYP and ωB97X) gives suitable results for compounds **2**-**6**. All methods underestimate β_{HRS} of compound **1** in its merocyanine form, and in all cases, the HF method underestimates β_{HRS}, from 60% (**1**) to 37% (**5**).

Turning now to the contrasts, the BLYP, B3LYP, and M06 XC functionals can strongly underestimate or overestimate the β_{HRS} contrasts. A clear improvement is

achieved when using the M06-2X, LC-BLYP, and ωB97x functionals, at least for compounds **2–4,** but a similar performance is achieved at the HF level. None of the methods is suitable to describe the β_{HRS} contrasts of compounds **5** and **6**, highlighting the difficulty in selecting a priori an XC functional to assess a broad variety of chromophores having second-order NLO responses.

Acknowledgements This work was supported by funds from the Belgian Government (IUAP N° P7/5 "Functional Supramolecular Systems") and the Francqui Foundation. It has also been done in the frame of the Centre of Excellence LAPHIA (Investments for the future: Programme IdEx Bordeaux–LAPHIA (ANR-10-IDEX-03-02)). V.L. thanks the Fund for Scientific Research (F.R.S.-FNRS) for his Research Associate position and M.H.C. the IUAP N° P7/5. The calculations were performed on the computing facilities of the Consortium des Équipements de Calcul Intensif (CÉCI, http://www.ceci-hpc.be), including those of the Technological Platform of High Performance Computing, for which we gratefully acknowledge the financial support of the FNRS-FNRC (Conventions 2.4.617.07.F and 2.5020.11) and of the University of Namur as well as on the "Mésocentre de Calcul Intensif Aquitain" (MCIA) of the University of Bordeaux, financed by the Conseil Régional d'Aquitaine and the French Ministry of Research and Technology.

References

1. D.P. Shelton, J.E. Rice, Chem. Rev. **94**, 3–29 (1994)
2. T. Verbiest, K. Clays, V Rodriguez, *Second-Order Nonlinear Optical Characterization Techniques: An Introduction* (Taylor & Francis, 2009)
3. D.R. Kanis, M.A. Ratner, T.J. Marks, Chem. Rev. **94**, 195–242 (1994)
4. J.L. Brédas, C. Adant, P. Tackx, A. Persoons, B.M. Pierce, Chem. Rev. **94**, 243–278 (1994)
5. P.J. Campagnola, L.M. Loew, Nat. Biotechnol. **21**, 1356–1360 (2003); Y.C. Liang, A.S. Dvornikov, P.M. Rentzepis, Proc. Natl. Acad. Sci. USA **100**, 8109–8112 (2003)
6. P.C. Ray, Chem. Rev. **110**, 5332–5365 (2010)
7. R. Bersohn, Y.H. Pao, H.L. Frisch, J. Chem. Phys. **45**, 3184–3198 (1966)
8. S.Y. Liu, C.E. Dykstra, J. Phys. Chem. **91**, 1749–1754 (1987)
9. G.J.B. Hurst, M. Dupuis, E. Clementi, J. Chem. Phys. **89**, 385–395 (1988)
10. S. Yamada, M. Nakano, I. Shigemoto, S. Kiribayashi, K. Yamaguchi, Chem. Phys. Lett. **267**, 445–451 (1997)
11. T. Pluta, A.J. Sadlej, Chem. Phys. Lett. **297**, 391 (1998); A. Baranowska, A.J. Sadlej, J. Comput. Chem. **31**, 552–560 (2010); R. Zalesny, A. Baranowska-Laczkowska, M. Medved, J.M. Luis, J. Chem. Theor. Comput. **11**,4119-4128 (2015)
12. G. Maroulis, J. Chem. Phys. **108**, 5432–5448(1998); G. Maroulis, Theor. Chem. Acc. **129**,437–445 (2011)
13. R.A. Kendall, T.H. Dunning Jr., R.J. Harrison, J. Chem. Phys. **96**, 6796–6806(1992); D.E. Woon, T.H. Dunning Jr., J. Chem. Phys. **100**, 2975–2988 (1994)
14. F. Castet, E. Bogdan, A. Plaquet, L. Ducasse, B. Champagne, V. Rodriguez, J. Chem. Phys. **136**, 024506 (2012)
15. F.D. Vila, D.A. Strubbe, Y. Takimoto, X. Andrade, A. Rubio, S.G. Louie, J.J. Rehr, J. Chem. Phys. **133**, 034111 (2010)
16. J.D. Talman, Phys. Rev. A **86**, 022519 (2012)
17. H.D. Cohen, C.C.J. Roothaan, J. Chem. Phys. **43**, S34 (1965)
18. D.M. Bishop, S.A. Solunac, Chem. Phys. Lett. **122**, 567 (1985)
19. A.A.K. Mohammed, P.A. Limacher, B. Champagne, J. Comput. Chem. **34**, 1497–1507 (2013)

20. M. de Wergifosse, V. Liégeois, B. Champagne, Int. J. Quantum Chem. **114**, 900–910 (2014)
21. J. Linderberg, Y. Öhrn, *Propagators in Quantum chemistry* (Wiley-Interscience, Hoboken, 2004)
22. T. Helgaker, S. Coriani, P. Jørgensen, K. Kristensen, J. Olsen, K. Ruud, Chem. Rev. **112**, 543 (2012)
23. S. Karna, M. Dupuis, J. Comput. Chem. **12**, 487 (1991)
24. S.J.A. van Gisbergen, J.G. Snijders, E.J. Baerends, J. Chem. Phys. **109**, 10657 (1998)
25. P. Beaujean, B. Champagne, J. Chem. Phys. **145**, 044311 (2016)
26. H. Sekino, R.J. Bartlett, J. Chem. Phys. **94**, 3665 (1991)
27. J.E. Rice, N.C. Handy, J. Chem. Phys. **94**, 4959 (1991)
28. M. de Wergifosse, F. Castet, B. Champagne, J. Chem. Phys. **142**, 194102 (2015)
29. P. Kaatz, E.A. Donley, D.P. Shelton, J. Chem. Phys. **10**, 849 (1998)
30. J.F. Ward, C.K. Miller, Phys. Rev. A **19**, 826 (1979)
31. D.P. Shelton, J. Chem. Phys. **137**, 044312 (2012)
32. D.M. Bishop, F.L. Gu, S.M. Cybulski, J. Chem. Phys. **109**, 8407 (1998)
33. F. Castet, B. Champagne, J. Chem. Theor. Comput. **8**, 2044 (2012)
34. P. Karamanis, R. Marchal, P. Carbonnière, C. Pouchan, J. Chem. Phys. **135**, 044511 (2012)
35. K.Y. Suponitsky, S. Tafur, A.E. Masunov, J. Chem. Phys. **129**, 044109 (2008)
36. M. de Wergifosse, B. Champagne, J. Chem. Phys. **134**, 074113 (2011)
37. S.I. Lu, C.C. Chiu, Y.F. Wang, J. Chem. Phys. **135**, 134104 (2011)
38. H. Sun, J. Autschbach, ChemPhysChem **14**, 2450–2461 (2013)
39. K. Garrett, X.A. Sosa Vazquez, S.B. Egri, J. Wilmer, L.E. Johnson, B.H. Robinson, C.M. Isborn, J. Chem. Theory Comput. **10**, 3821–3831 (2014)
40. J. Tomasi, B. Mennucci, R. Cammi, Chem. Rev. **105**, 2999–3094 (2005)
41. J.L. Oudar, D.S. Chemla, J. Chem. Phys. **66**, 2664–2668 (1977)
42. P. Kaatz, D.P. Shelton, Mol. Phys. **88**, 683–691 (1996)
43. K. Coutinho, S. Canuto, Adv. Quantum Chem. **28**, 89–105 (1997)
44. K. Coutinho, R. Rivelino, H.C. Georg, S. Canuto, in *Solvation Effects in Molecules and Biomolecules: Computational Methods and Applications* (Springer, 2008), pp. 159–189
45. M. Hidalgo Cardenuto, B. Champagne, Phys. Chem. Chem. Phys. **17**, 23634–23642 (2015)
46. M. Hidalgo Cardenuto, F. Castet, B. Champagne, RSC Adv. **6**, 99558–99563 (2016)
47. E. Deniz, J. Cusido, S. Swaminathan, M. Battal, S. Impellizzeri, S. Sortino, F.M. Raymo, J. Photochem. Photobiol., A **229**, 20–28 (2012)
48. M. Kamiya, H. Sekino, T. Tsuneda, K. Hirao, J. Chem. Phys. **122**, 234111 (2005); F. Bulat, A. Toro-Labbé, B. Champagne, B. Kirtman, W. Yang, J. Chem. Phys. **123**, 014319 (2005)
49. B. Champagne, K. Kirtman, J. Chem. Phys. **125**, 024101 (2006)
50. B. Champagne, E.A. Perpète, D. Jacquemin, S.J.A. van Gisbergen, E.J. Baerends, C. Soubra-Ghaoui, K.A. Robins, B. Kirtman, J. Phys. Chem. A **104**, 4755–4763 (2000)
51. L. Kronik, T. Stein, S. Refaely-Abramson, R. Baer, J. Chem. Theory Comput. **8**, 1515–1531 (2012)
52. B.J. Coe, Chem. Eur. J. **5**, 2464–2471 (1999); J.A. Delaire, K. Nakatani K, Chem. Rev. **100**, 1817–1845 (2000); I. Asselberghs, K. Clays, A. Persoons, M.D. Ward, J. McCleverty, J. Mater. Chem. **14**, 2831–2839 (2004); F. Castet, V. Rodriguez, J.L. Pozzo, L. Ducasse, A. Plaquet, B. Champagne, Acc. Chem. Res. **46**: 2656–2665 (2013)
53. A. Plaquet, M. Guillaume, B. Champagne, F. Castet, L. Ducasse, J.L. Pozzo, V. Rodriguez, Phys. Chem. Chem. Phys. **10**, 3223–3232 (2008)
54. A. Plaquet, B. Champagne, J. Kulhanek, F. Bures, E. Bogdan, F. Castet, L. Ducasse, V. Rodriguez, ChemPhysChem **12**, 3245–3252 (2011)
55. A. Plaquet, B. Champagne, F. Castet, L. Ducasse, E. Bogdan, V. Rodriguez, J.L. Pozzo, New J. Chem. **33**, 1349–1356 (2009)
56. E. Bogdan, A. Plaquet, L. Antonov, V. Rodriguez, L. Ducasse, B. Champagne, F. Castet, J. Phys. Chem. C **114**, 12760–12768 (2010)
57. A. Plaquet, B. Champagne, L. Ducasse, E. Bogdan, F. Castet, AIP Conf. Proc. **1642**, 481–487 (2015)